New Insight into the Peroxidase−Hydroxamic Acid Interaction Revealed by the Combination of Spectroscopic and Crystallographic Studies†

Chiara Indiani,‡ Elisa Santoni,‡ Maurizio Becucci,§ Alberto Boffi,|| Keiichi Fukuyama,⊥ and Giulietta Smulevich*,‡

Dipartimento di Chimica, Universita' di Firenze, Polo Scientifico, Via della Lastruccia 3, I-50019 Sesto Fiorentino (FI), Italy, LENS−European Laboratory for Nonlinear Spectroscopy, Polo Scientifico, Via N. Carrara 1, I-50019 Sesto Fiorentino (FI), Italy, Department of Biochemical Sciences, University "La Sapienza" 00185 Rome, Italy, and Department of Biology, Graduate School of Science, Osaka University, Toyonaka, Osaka 560-0043, Japan

Received July 22, 2003

ABSTRACT: Aromatic hydroxamic acids, such as salicylhydroxamic (SHA) and benzohydroxamic (BHA) acids, are commonly used as probes for studying the active sites of peroxidases. In this paper, we have extended the study of the complexes of *Arthromyces ramosus* peroxidase (ARP/CIP) with BHA and SHA by analyzing their Raman spectra in solution and in single crystals. The experiments were carried out under various conditions to identify the best experimental conditions, and hence, avoid artifacts deriving from the preparation of the samples or collection of the spectra. The analysis of the data takes also into account the characteristic of the electronic absorption spectra in solution and the crystal structures of the complexes. The results showed small differences between the solution and the crystal phases even though the coordination state can be dramatically affected by the physical or chemical conditions. The greater sensitivity of the spectroscopic technique enabled us to establish the existence of multiple species upon complexation of the protein with the hydroxamic acids that could not be detected by ordinary X-ray crystallography. Furthermore, SHA titration experiments and singular value decomposition analysis of the absorption spectra indicated the presence of two binding sites in the protein, one with a high affinity (K_d = 1.7 mM), which should correspond to the SHA bound protein as determined by X-ray, and the other with a very low affinity (K_d > 80 mM) probably located in a non-heme site. This suggests that the heterogeneous titration line shape involves ligand binding to a non-heme site in competition with the canonical heme site. In contrast, the titration profile obtained with the BHA ligand is monophasic, in agreement with all the peroxidases so far studied.

The binding of non-physiological substrates, such as aromatic hydroxamic acids, to peroxidases has been extensively investigated with the aim of probing the aromatic donor binding site. In particular, recent X-ray structures have been solved for the complexes between horseradish peroxidase (HRPC) and benzohydroxamic acid (BHA) (*1*), *Arthromyces ramosus* peroxidases (ARP) (since *Coprinus cinereus* (CIP) and *Arthromyces ramosus* peroxidases are identical both in its covalent structure and enzymatic properties (*2*, *3*), we will refer to this peroxidase by the name ARP/CIP) with both BHA (*4*) and salicylhydroxamic acid (SHA) (*5*) and myeloperoxidase (MPO) with SHA (*6*). Comparison between the structures of the ARP/CIP-BHA (*4*) and ARP/CIP-SHA (*5*) complexes reveals that the location of the aromatic rings in the active site is similar. They are nearly parallel to the heme plane and located in the distal cavity. The hydroxamic acid moiety forms hydrogen bonds with the conserved distal His55 (CIP numbering), Arg51, and Pro153 residues. The additional hydroxyl group of SHA relative to BHA does not form hydrogen bonds with any amino acid residue in the heme cavity. In HRPC, the bound BHA molecule forms an extensive hydrogen bonding network with the same distal catalytic residues His, Arg, and Pro. In addition, a hydrophobic pocket surrounding the aromatic ring of the substrate was found in HRPC, which is not present in ARP/CIP (*1*). The aromatic molecule does not bind directly to the heme iron, but the addition of SHA or BHA to HRPC and ARP/CIP displaces water molecules from the distal cavity leaving only one molecule of water close to the heme iron. The iron−water distances in the HRPC-BHA, ARP/CIP-BHA, and ARP/CIP-SHA complexes were found to be 2.6 (*1*), 2.7 (*4*), and 2.8 Å (*5*), respectively. Considering the rather long Fe−H_2O distance, there have been conflicting interpretations concerning the extent to which BHA affects the binding of the water molecule to the Fe atom. On the basis of electronic absorption (*7*), resonance Raman (*8*−*11*), and EPR (*12*), it was concluded that the BHA complex of HRPC has a water bound to the Fe atom, whereas NMR proton hyperfine shifts indicated that the HRPC-BHA

† This work was supported by the Italian Consiglio Nazionale delle Ricerche (CNR) and Ministry of Education, Universities, and Research (MIUR) (PRIN MMO3185591) (G.S.) and EU HPRI CT 1999 00111) (M.B.). Part of this work was done with the approval of the Photon Factory Advisory Committee (Proposal 99G303).

* To whom correspondence should be addressed. E-mail: giulietta.smulevich@unifi.it.

‡ Universita' di Firenze.

§ LENS−European Laboratory for Nonlinear Spectroscopy.

|| University "La Sapienza".

⊥ Osaka University.

10.1021/bi035290l CCC: $25.00
Published on Web 11/04/2003

complex was a 5 coordinate high spin (5c HS) species (*13*). Very recently, the spectroscopic data acquired for the proteins in solution indicated that the binding of BHA to both HRPC (*14*) and ARP/CIP (*15*, *16*) induces the formation of a 6 coordinate high spin (6c HS) species that, on the basis of the comparison of the resonance Raman (RR) spectra of single crystal and solution samples of the HRPC-BHA complex, was demonstrated to derive from a water molecule bound to the heme iron (*15*). However, the solution spectra for HRPC and ARP/CIP complexed with BHA differ in terms of the amount of the 6c form present. At relatively low ligand concentration, the former protein fully converts from the resting 5c to the 6c state upon addition of the aromatic donor (*15*), whereas ARP/CIP is not fully converted (*16*). This difference might be correlated with the small variation observed by X-ray crystallography in the iron−water distance between HRPC-BHA (2.6 Å), ARP/CIP-BHA (2.7 Å), and ARP/CIP-SHA (2.8 Å), which are longer than the usual iron−ligand distance (2.1 Å). The increased distance could correspond to higher proportion of the 5c HS heme in equilibrium with the 6-aquo. However, the accuracy of the distance between the heme iron and the ligand is generally limited (0.2 Å) in the X-ray determination (*5*). A more detailed study of the correlation between the iron−ligand distance and the electronic structure for a given ligand is possible by spectroscopy. In particular, comparison of detailed Raman spectra for complexes in crystal and solution forms provides a means of bridging crystallographic and solution studies (*17*, *18*).

In this paper we, therefore, extended the study of the complexes of ARP/CIP with BHA and SHA by analyzing their Raman spectra in solution and in single crystals. The experiments were carried out under various experimental conditions to avoid artifacts deriving from the preparation of the samples or collection of the spectra.

MATERIALS AND METHODS

Sample Preparation. Recombinant CIP was obtained by expression in transformed *Aspergillus oryzae* (*19*) and purified as previously described (*20*). The fungal peroxidase ARP was isolated from extracellular culture medium of *A. ramosus* (*21*) and purified as previously described (*22*).

The following buffers were used: 20 mM sodium acetate at pH 5.5, 10 mM phosphate or 10 mM MOPS (4-morpholinepropanesulfonic acid) at pH 7.0, and 12 mM Tris/HCl at pH 8.0. All the buffers contain 1 mM $CaCl_2$. Where necessary, ammonium sulfate (Merck) was added. The concentrations of the protein in the resting state were calculated from the absorbance using the extinction coefficient 109 mM^{-1} cm^{-1} at 405 nm (*23*). The concentration range was 3−60 μM for both electronic absorption and RR measurements.

The complexes with benzohydroxamic acid (BHA Sigma) and salicylhydroxamic acid (SHA Merck) were made by the addition of ligand solutions to the proteins to give a final concentration corresponding to ca. 85% protein saturation for the ARP/CIP-BHA complex and about 80% protein saturation for the ARP/CIP-SHA complex, due to the low solubility of SHA.

Single crystals of ARP, with and without BHA and SHA, containing 33% saturated ammonium sulfate in the soaking solution were obtained as previously reported (*4*, *5*, *21*). The ARP-BHA crystals without ammonium sulfate were prepared by soaking the native ARP crystals first in 50 mM sodium acetate buffer (pH 5.5) containing saturated sodium sulfate for 1 h, and then in a solution containing 25 mM BHA for 4 h. The crystals were sealed in glass capillaries with a trace amount of the soaking solution. The crystals belong to the space group $P4_22_12$ with $a = b = 74.5$ Å and $c = 117.1$ Å.

Table 1: Summary of Crystallographic Data and Refinement

(a) Conditions and Results of Data Collection

	data set 1	data set 2
wavelength (Å)	1.5418	1.00
oscillation angle/frame (deg)	1.2	1.0
no. of frames	75	90
resolution limit (Å)	1.9	1.6
measured reflections	167454	302833
independent reflections	26415	38678
completeness (%)[a]	98.7 (95.2)	89.7 (93.2)
R_{merge} (%)[a,b]	5.7 (24.8)	4.5 (22.6)

(b) Results of Crystallographic Refinement

resolution range (Å)	7.0−1.7
R factor/R_{free} (%)[c]	16.9/22.1
no. of reflections ($F > 2\sigma_F$)	33673
no. of atoms refined[d]	2807 (248)
r.m.s. deviations from ideality	
bond lengths (Å)	0.014
bond angles (deg)	2.5
Ramachandran plot	
most favored regions (%)	91.3
additional allowed regions (%)	8.7

[a] The values in parentheses refer to the highest resolution shell. [b] $R_{merge} = \sum_{hkl}\sum_i |I_i(hkl) - \langle I(hkl)\rangle| / \sum_{hkl}\sum_i I_i(hkl)$. [c] R_{free} was calculated for 5% reflections randomly excluded from the refinement. [d] The value in parentheses is the number of water molecules.

Crystallographic Measurements and Data Processing. Two sets of diffraction data were collected at room temperature; the first set was collected on an R-AXIS IV imaging plate area detector using CuKα radiation generated by a Rigaku rotating anode (or Rigaku ultra ×18), the second set with ADSC Quantum 4 CCD detector and synchrotron radiation at BL18B, Photon Factory. Diffraction images were processed with MOSFLM (*24*), and the integrated intensities were scaled for each set with SCALA (*25*). Conditions and results of data collection are given in Table 1a.

Crystallographic Refinement. The atomic parameters of ARP at pH 5.5 (*26*) were used as the starting model, in which several water molecules on the distal side of the heme were excluded. The structure was refined by the program XPLOR (*44*) and checked by the ($2F_o - F_c$) and ($F_o - F_c$) maps with TURBO-FRODO (*27*). In the initial stage of the refinement, the structure was refined using each set of intensity data. Each map revealed the electron density corresponding to the BHA molecule, and the two sets of intensity data were merged and scaled ($R_{merge} = 3.0\%$ in F) using a program based on the method described by Hamilton and co-workers. (*28*). This allowed high resolution data lacking in set 1 and covered relatively low completeness in set 2. The refinement was continued with the merged intensity data. Conformations of side chains for several residues were revised, and the recently identified carbohydrate bonded to Ser339 and BHA molecule was included. The final R factor and R_{free} are 16.9 and 22.1%, respectively, for the reflections in the 7.0−1.7 Å resolution range. Results

Table 2: Binding of Benzohydroxamic (BHA) and Salicylhydroxamic (SHA) Acids to Resting State ARP/CIP and HRPC at Various pH Values

	hydroxamic acid dissociation constant (K_d, mM)				
peroxidase	pH 5.0	pH 5.5	pH 6.0	pH 7.0	pH 7.4
ARP/CIP-BHA		2.9			3.2 (*5*)
ARP/CIP-SHA		1.7 >80			3.2 (*5*)
HRPC-BHA	0.0033 (*35*)		0.0024 (*7*) 0.0023 (*35*)	0.0025 (*35*)	0.0046 (*5*)
HRPC-SHA	0.0092 (*35*)		0.0078 (*7*) 0.0077 (*35*)	0.011 (*35*)	0.17 (*5*)

[a] The numbers in parentheses indicate the appropriate references.

of crystallographic refinement are given in Table 1b. The coordinates have not been submitted to the Protein Data Bank, as the structure is identical to that previously reported (1HSR).

Binding of Aromatic Hydroxamic Acids. SHA and BHA titrations were carried out at about 25°C by making successive additions of a BHA or SHA stock solution to a solution of ARP/CIP (4−7 μM in buffer, 2.5 mL) to a final ligand concentration of about 16 mM. All data were corrected for the dilution upon substrate addition. In addition, since at high SHA concentration SHA absorption in the Soret region is not negligible, the absorption spectra of SHA were subtracted from the absorption spectra of CIP-SHA complex. The data matrix of the spectra obtained in the titrations has been deconvolved with the Singular Value Decomposition (SVD) algorithm (*29*) to remove noise and identify the presence of possible spectral intermediates. The SVD procedure entails transformation of the data set, **A**, into the product of three matrixes $\mathbf{A} = USVT$, where the U columns are the orthonormal basis spectra, the V column (eigenvectors) represents the amplitudes corresponding to the basis spectra as a function of ligand concentration, and the diagonal matrix S (singular values) provides the relative contribution of the basis spectra to the observed signal. The first two basis spectra and the corresponding two V columns were sufficient to account for the whole spectral trend as a function of ligand concentration, thereby confirming the presence of only two spectral species (i.e., an unliganded species and a ligand bound species). The titration profiles thus obtained (V columns) were fitted either to a canonical single site equilibrium titration curve (in the case of BHA) or to two independent ligand binding sites (in the case of SHA) by a least-squares method. The procedure was carried out by standard algorithms provided within the software Matlab 5.0 (The Math Works Inc., South Natick, MA) on a IBM PC.

Spectroscopy. *Solution*. The absorption spectra were recorded with a Cary 5 spectrophotometer in quartz cuvettes (1 cm optical path) for the titration experiments and in NMR tubes prior and after the resonance Raman experiments. No degradation was observed under the experimental conditions used. The RR spectra in solution were obtained with excitation from the 406.7 and 413.1 nm lines (the unligated CIP enzyme was found to be very unstable at 406.7 nm excitation (*19*)) of a Kr^+ laser (Coherent Innova/K) and the 514.5 nm line of an Ar^+ laser (Coherent Innova/90). For the spectra recorded with Soret excitation (406.7 nm), the backscattered light from a slowly rotating NMR tube was collected and focused into a computer-controlled double monochromator (Yobin Yvon HG2S) equipped with a cooled photomultiplier (RCA C31034 A) and photon-counting electronics. To minimize heating effects induced on the protein by the laser beam, the room-temperature RR spectra were collected using a rotating NMR tube cooled by a gentle flow of N_2 gas passed through liquid N_2. For the spectra recorded with visible excitation, the same apparatus reported for the crystals was used.

Single Crystals. The crystals were sealed in 0.7 mm glass capillaries with a trace amount of the soaking solution. A Raman microprobe apparatus reported previously (*30*) was used. It consists of an Olympus BHSM2 microscope equipped with an extra-long working distance Nikon M Plan achromatic objective capable of 60× magnification with a 0.70 numerical aperture. The spectrometer, a HR460 Jobin-Yvon monochromator, has a 1800 grooves/mm grating and an ultimate resolving power exceeding 10^4 at 550 nm. The detector is a liquid nitrogen-cooled Spectraview 2D CCD head of 578 × 375 pixels that enabled the simultaneous recording of a 450 cm^{-1} spectral region in our spectrometer. To obtain a reasonable signal-to-noise ratio, a 200 μm slit was used, giving a 5 cm^{-1} spectral resolution. The laser power on the crystal surface is reported in each figure caption. The RR spectra were obtained with the 514.5 nm line of an Ar^+ laser (Coherent Innova/90) at room temperature. The RR spectra were calibrated with indene as standard. The frequencies were accurate to ± 1 cm^{-1} for the intense isolated bands and about ± 2 cm^{-1} for overlapped bands or shoulders.

RESULTS AND DISCUSSION

Binding of Aromatic Hydroxamic Acids. Table 2 compares the BHA and SHA dissociation constants (K_d) for ARP/CIP and HRPC, obtained between pH 7.4 and 5.5. It is evident that BHA binds HRPC 3 orders of magnitude stronger than ARP/CIP, probably as a result of extra hydrophobic contacts that are lacking in ARP/CIP, namely, various phenylalanine residues (Phe68, Phe179, Phe142) *(1, 31−34)*. No substantial changes have been observed for the dissociation constants of the BHA complexes upon changing pH, whereas a marked decrease is observed for both ARP/CIP-SHA and HRPC-SHA complexes at the lower pH value. As noted by Schonbaum (*7*), hydroxamate anions do not associate with peroxidase enzymes; therefore, the pK_a of the aromatic hydroxamic acids must be considered to evaluate the ligand binding. The pK_a of BHA is 8.8 (*7*), and the pK_a values determined for SHA are 7.4 and 10.0. The pH value at 7.4 is assigned to the hydroxamic acid groups and the second to the ring hydroxyl (*35*). The decrease of the K_d value observed

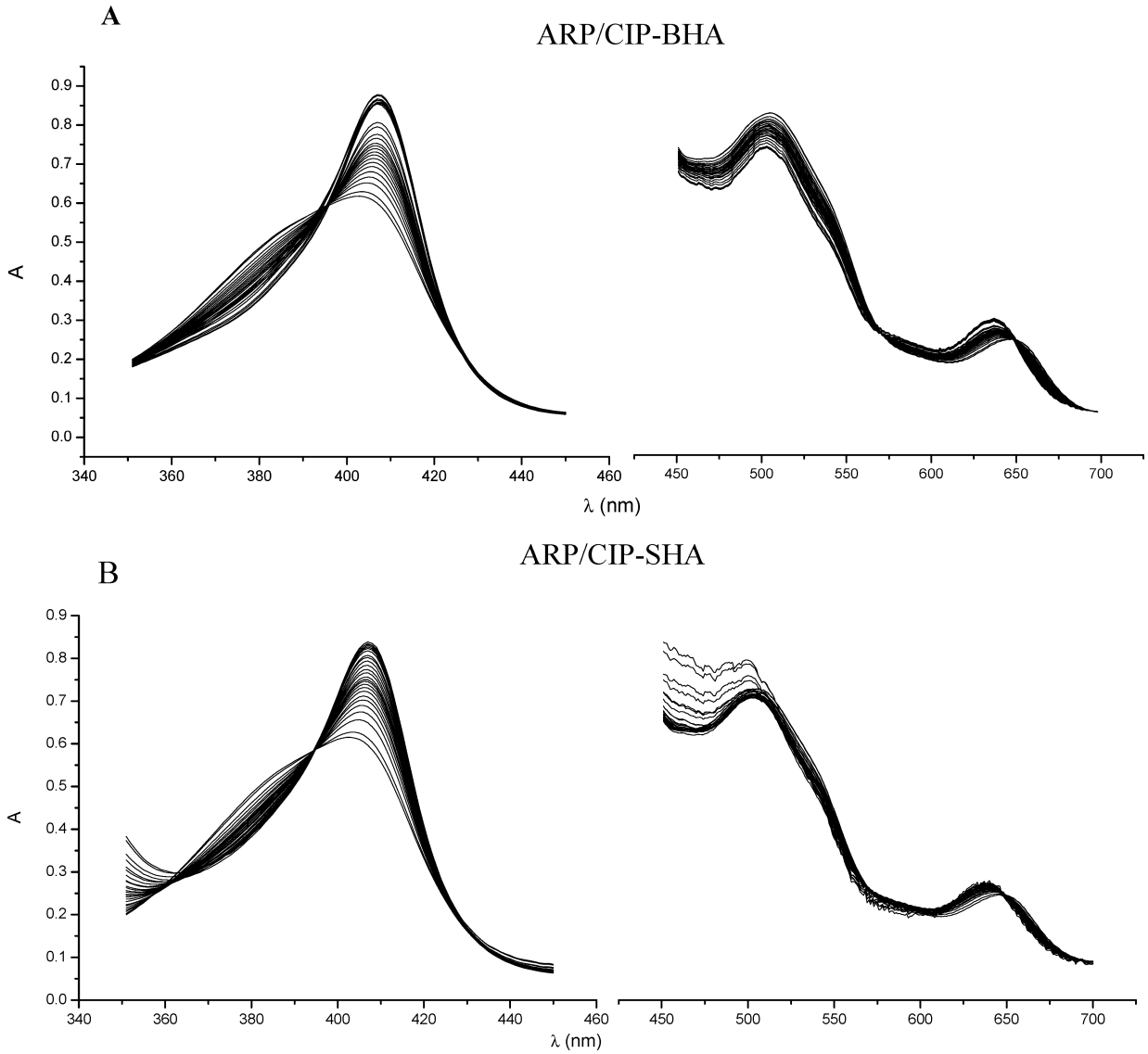

FIGURE 1: Spectral changes in the UV−vis absorption region accompanying BHA (A) and SHA (B) binding to ARP/CIP at pH 5.5. Titrations were carried out at room temperature by making successive additions of hydroxamic acid stock solution (20 mM) to a solution of the enzyme (4−7 μM) to a final hydroxamic acid concentration of ca. 16 mM. All the spectra are corrected for dilution following substrate addition.

for the ARP/CIP-SHA and HRPC-SHA complexes upon lowering the pH from pH 7.4 to 5.5 (*5*, *7*, *35*) reflects the equilibrium between the protonated−unprotonated forms of SHA in solution. Since the proteins bind the neutral form of the hydroxamic acids (*35*), hereafter only the K_d values we have obtained for the ARP/CIP-BHA and -SHA complexes at pH 5.5 will be considered.

Figure 1 shows the spectral changes in the UV−vis absorption region accompanying BHA (Figure 1A) and SHA (Figure 1B) binding to resting ARP/CIP in solution at pH 5.5. Prior to complexation, the protein displays typical properties of a 5c heme (i.e., Soret maximum at 403 nm with an intense shoulder at lower wavelength, β band at 505 nm, and CT1 band at 647 nm (*20*)). Upon addition of either BHA or SHA, the electronic absorption spectrum shows marked changes. The Soret band red-shifts and sharpens with an increase of the extinction coefficient by about 35%, the shoulder at lower wavelength disappears, and the CT1 band blue-shifts from 647 to 640 (ARP/CIP-SHA) and 638 nm (ARP/CIP-BHA). All these changes, similar to those already reported for the ARP/CIP-BHA adduct at pH 7.0 (*36*, *37*), are consistent with the formation of an aquo 6c species. Isosbestic points observed at 394 and 648 nm indicate the presence of an equilibrium between two species, the resting 5c and the bound 6c species. Figure 2 shows the ligand binding isotherms of ARP/CIP with BHA (Figure 2A) and SHA (Figure 2B,C). In Figure 2A and B, the ARP/CIP-BHA and ARP/CIP-SHA titration data are fitted to a single binding site reaction scheme. Inspection of the fitting profile of Figure 2B, however, shows that convergence is not obtained toward the higher asymptote suggesting that a more complex equilibrium ligand binding behavior must be taken into account to describe SHA binding to ARP/CIP. Analysis of the spectral line shapes (Figure 3), carried out by the SVD procedure, also indicates that in ARP/CIP-SHA, only two spectrally distinct species contribute to the observed signal (i.e., the 5c species and the high spin 6c derivative mentioned previously). In other words, each spectrum of the titration shown in Figure 1B is a linear combination of the 5c and 6c species with no intermediate(s). The spectra reconstructed

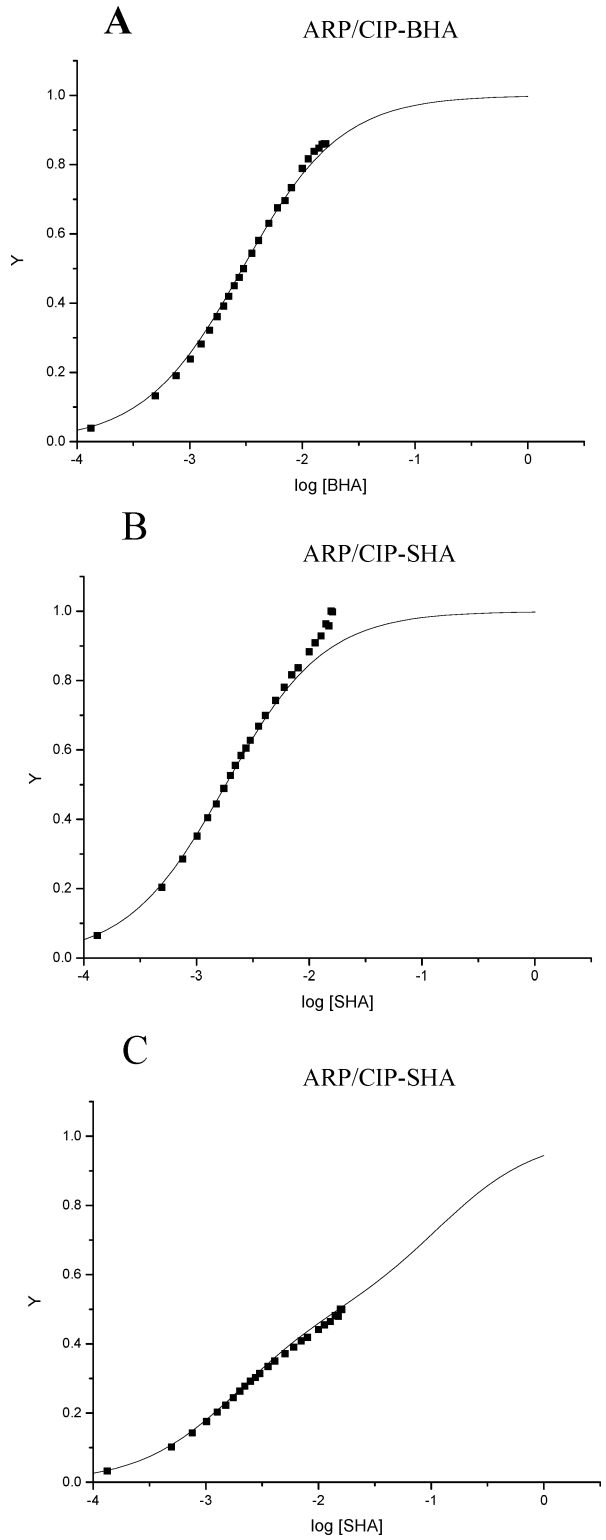

FIGURE 2: Ligand binding isotherms of ARP/CIP with BHA (A) and SHA (B and C) showing the saturation fraction vs logarithm of the ligand concentration. (A and B) Continuous lines represent fitting curves obtained by minimizing the experimental data to a single binding site reaction; (C) the experimental points were obtained from a linear combination of the first two *V* columns by using the same coefficients obtained from the fitting of the spectral line shape of Figure 3. Continuous line in panel C represents the fitting curve obtained assuming two distinct binding sites.

with the SVD procedure indicate unambiguously that the last spectrum of the titration, at the highest SHA concentration (16 mM), is far from being a pure 6c fully ligand saturated

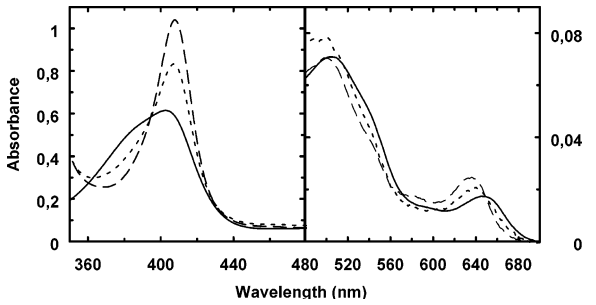

FIGURE 3: Spectral line shapes obtained from SHA titration of ARP/CIP. The absorption spectra of unbound (continuous line) and fully bound (dashed line) ARP/CIP are compared with the spectrum obtained at 16 mM SHA concentration (dotted line), corresponding to the last spectrum in the titration profile depicted in Figure 1B. The fully bound spectrum has not been obtained by experiments but was extrapolated and fitted as a linear combination of the two basis spectra obtained from the SVD procedure (see Materials and Methods). The two coefficients of the linear combination were minimized by least-squares method.

species but approaches to about 60% saturation. Thus, the SHA ligand binding process to ARP/CIP entails at least a two step process within a single spectral transition. Such heterogeneous ligand binding behavior is not unusual and has also been reported in the case of several bacterial hemoglobins where an explicit reaction scheme that involves the presence of two protein conformations has been taken into account (*38*). In the present case, experimental evidence for the presence of distinct conformers has not been obtained. Thus, the ligand binding profile has been analyzed in terms of two independent processes in the framework of a minimal scheme that takes into account two apparent binding constants (see Materials and Methods). At low ligand concentration, a K_d of 1.7 mM was found, whereas at high ligand concentration, the K_d was >80 mM. In contrast, a simple single site titration profile is observed in the case of ARP/CIP-BHA ($K_d = 2.9$ mM). Therefore, at higher ligand concentrations, SHA begins to occupy a second site that has a lower affinity ($K_d > 80$ mM). Binding of SHA to this site does not alter the spin and coordination state of the heme iron with respect to the resting protein, suggesting that this is a non-heme site. Thus, the amount of 6c form detected by the spectroscopic method cannot be indicative of the total amount of SHA bound to the protein. To our knowledge, a second binding site has not been observed either for SHA or for BHA in HRPC.

Interestingly, unlike HRPC (*7*), in ARP/CIP the affinity of the heme site for SHA is slightly higher ($K_d = 1.7$ mM) than for BHA ($K_d = 2.9$ mM), as is also evident from the absorption spectrum of the ARP/CIP-SHA adduct that at very low ligand concentrations (up to 1.2 mM) shows a slightly larger quantity of 6c species than CIP-BHA (data not shown). Recently, it has been shown that the binding of BHA to HRPC is enthalpy driven at pH 6.0−7.0, with the hydrogen bond to the distal Arg38 providing the largest contribution to the binding energy. The overall relatively weak binding of SHA to HRPC (Table 2) is due to large entropic barriers around neutral pH, with the distal Arg38 acting as an entropic gate barrier (*35*). However, these findings do not apply to ARP/CIP since the X-ray structures of both the ARP/CIP-BHA (*4*) and ARP/CIP-SHA (*5*) are quite similar, including the hydrogen bond distances between the hydroxamic acid groups and the distal His, Arg, and Pro residues. Comparing

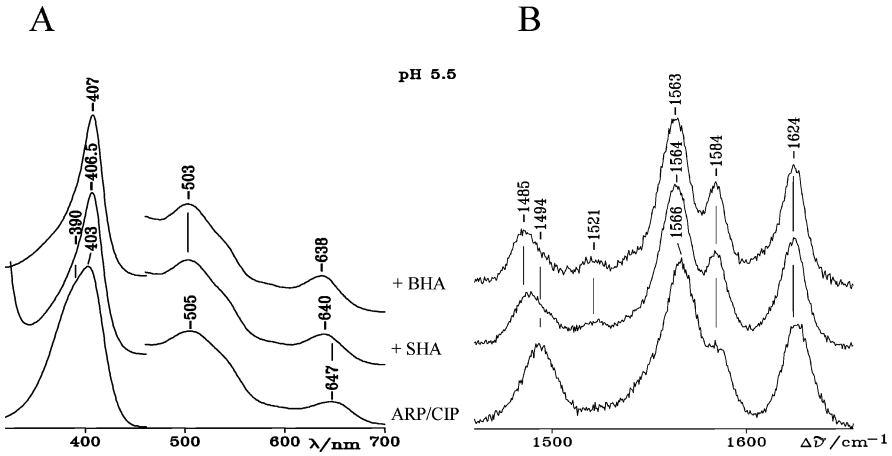

FIGURE 4: Coordination and spin states of ARP/CIP-BHA and -SHA complexes. (A) Electronic absorption spectra of ARP/CIP (6 μM), its complexes with SHA (3.7 μM ARP/CIP plus 7.7 mM SHA), and BHA (3.7 μM ARP/CIP plus 15.5 mM BHA) in 20 mM sodium acetate buffer, pH 5.5. The visible region is expanded 5-fold. (B) Corresponding resonance Raman spectra. Experimental conditions: 5 cm^{-1} spectral resolution; ARP/CIP, 413.1 nm excitation, 10 mW laser power at the sample, 15 s/0.5 cm^{-1} accumulation time; +SHA, 406.7 nm excitation, 15 mW laser power at the sample, 12 s/0.5 cm^{-1} accumulation time; +BHA, 406.7 nm excitation, 15 mW laser power at the sample, 9 s/0.5 cm^{-1} accumulation time.

these structures with that of the HRPC-BHA (*1*), the only marked difference is found in the larger hydrogen bond distance between the carbonyl group of the hydroxamic acid and the distal Arg. The O···N distance is 3.3 Å in the complexes of ARP/CIP and 2.9 Å in HRPC. This difference probably derives from the location of the guanidinium group of the Arg, which is farther away from the iron atom in resting ARP/CIP (*26*) than in resting HRPC (*31*).

Coordination and Spin States of the ARP/CIP-BHA and -SHA Complexes. Figure 4 shows the electronic absorption (Figure 4A) and RR (Figure 4B) spectra taken with the Soret excitation at pH 5.5 of resting ARP/CIP and its complexes with SHA and BHA obtained at ligand concentrations corresponding to ca. 80−85% protein saturation. ARP/CIP-BHA and ARP/CIP-SHA are characterized by the presence of a different amount of unbound protein (as judged by the ν_3 band at 1494 cm^{-1}). The core size marker band frequencies of the 6c HS aquo form typical of the ARP/CIP-BHA complex have been previously shown to be at 1485 (ν_3), 1521 (ν_{38}), 1563 (ν_2), and 1584 cm^{-1} (ν_{37}) (*15*). The ARP/CIP-SHA adduct shows broad core size marker bands at frequencies between those of 5c and 6c HS hemes (ν_3 at 1488 cm^{-1} and ν_2 at 1564 cm^{-1}). They are due to the overlapping contribution of both 5c and 6c high spin species since the abundance of the 5c HS species is greater in the SHA complex as compared to the ARP/CIP-BHA complex as also confirmed by their electronic absorption spectra. In these spectra, in fact, the Soret band is slightly blue-shifted and shows a weak shoulder at about 390 nm, typical of the 5c HS heme (*18*); concomitantly, the CT1 band is 2 nm red-shifted as compared to the ARP/CIP-BHA spectrum and is broadened with a shoulder at 647 nm (Figure 4A).

The RR spectra taken with Soret excitation are consistent with the corresponding spectra recorded with visible excitation for the samples in solution and as a single crystal (Figure 5). The different excitations allow us to obtain a complete assignment of the different species. Using the Q-band excitation, the nontotally symmetric B_{1g} (depolarized) and A_{2g} (anomalous polarized) modes are enhanced via vibronic mixing (*39*), whereas the totally symmetric modes (polarized) are enhanced via the *A*-term in the Soret excitation. Figure

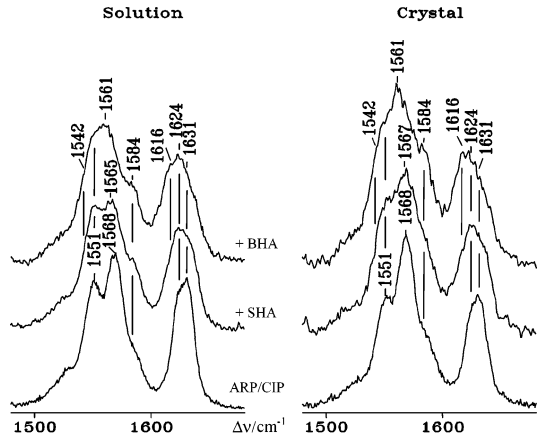

FIGURE 5: Comparison between solution (left) and single crystal (right) resonance Raman spectra of ARP/CIP, ARP/CIP-BHA, and ARP/CIP-SHA. Experimental conditions: 20 mM Na acetate buffer, 25 mM BHA or 12.5 mM SHA, pH 5.5; 514.5 nm excitation; 5 cm^{-1} spectral resolution. (Left) ARP/CIP, 2.3 mW laser power at the sample, 400 s accumulation time; BHA and SHA, 2.5 mW laser power at the sample, 1200 s accumulation time; (right) ARP/CIP, 10 μW laser power on the crystal surface, 8300 s accumulation time; BHA and SHA, 6 μW laser power on the crystal surface, 15 600 s accumulation time.

5 compares the RR spectra of solution and single crystal samples of the free ARP/CIP and its complexes with 12.5 mM SHA and 25 mM BHA at pH 5.5. It can be seen that there are no substantial differences in the band frequencies between the solution and the crystalline states. The ferric protein at pH 5.5 is a pure 5c HS as previously concluded (*26*, *40*). Upon addition of either BHA or SHA, changes in the frequency and relative intensities of the core size marker bands are observed. In the presence of BHA, the ARP/CIP spectra convert from a typical 5c HS (ν_{11} at 1551, ν_{19} at 1568, and ν_{10} at 1631 cm^{-1}) to a mainly 6c HS (ν_{11} at 1542, ν_{19} at 1561, and ν_{10} at 1616 cm^{-1}). In addition to the ligated form, a small amount of unbound 5c HS species is still present, as judged by the bands at 1631 cm^{-1} (ν_{10}) and the shoulder at 1551 cm^{-1} (ν_{11}), in agreement with previous studies (*15*, *16*). The ARP/CIP-SHA complex gives rise to spectra that are between those characteristic of the free and BHA ligated protein.

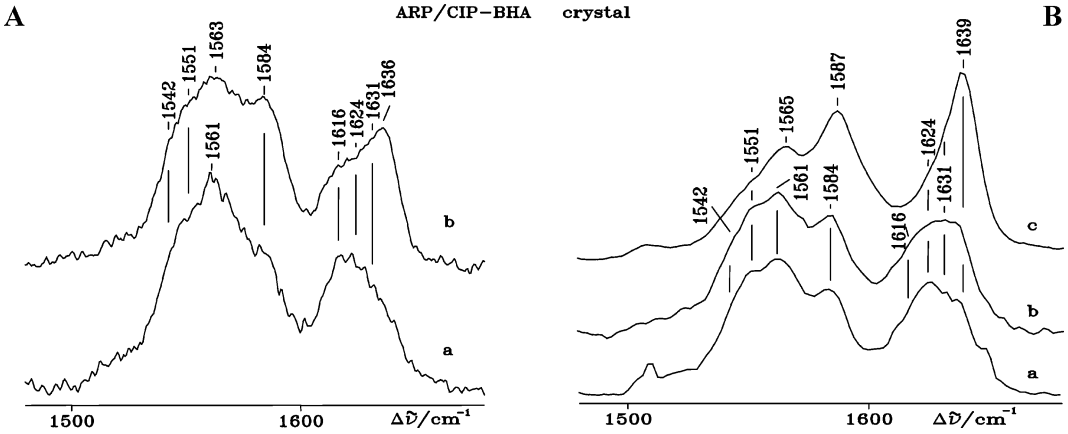

FIGURE 6: Effect of experimental conditions. (A) Resonance Raman spectra of ARP/CIP-BHA as a single crystal soaked in $(Na)_2SO_4$ (a) and in $(NH_4)_2SO_4$ (b). Experimental conditions: 514.5 nm excitation; 5 cm^{-1} spectral resolution; 6 μW laser power on the crystal surface, 15 600 s accumulation time. (B): Single crystal resonance Raman spectra of ARP/CIP-BHA soaked in $(NH_4)_2SO_4$ taken at different laser powers: (a) 100 μW laser power on the crystal surface, 720 s accumulation time; (b) 180 μW laser power on the crystal surface, 300 s accumulation time; and (c) 550 μW laser power on the crystal surface, 60 s accumulation time.

The RR spectra of the crystals are characterized by a striking enhancement of the inverse polarized ν_{19} mode at 1568 cm^{-1} (ARP/CIP), 1567 cm^{-1} (ARP/CIP-SHA), and 1561 cm^{-1} (ARP/CIP-BHA), which does not depend on the orientation of the crystal in the laser beam. This effect might derive from a larger ruffled distortion of the heme of the ARP crystal (*41*) with respect to the solution and be present also in the complexes (Shelnutt, personal communication).

Effect of Experimental Conditions. Proteins might be difficult to crystallize, and often the addition of salts or hydrophilic compounds in the crystallizing medium may help the crystallization process. However, the chemicals can modify the active site of the protein since the structural balance that determines the coordination state in a heme protein can be very delicate (*42*, *43*). Figure 6A shows the RR spectra of ARP/CIP-BHA for 514.5 nm excitation as a single crystal (a) obtained from a soaking solution containing Na_2SO_4 and (b) obtained from a soaking solution containing $(NH_4)_2SO_4$. Although the same experimental conditions were applied, it is evident that the presence of $(NH_4)_2SO_4$ induces the formation of a 6c low spin (LS) heme, as judged by the intensity increase of the bands at 1584 cm^{-1} (ν_{19}) and at 1636 cm^{-1} (ν_{10}). The same results were obtained for the ARP/CIP-SHA crystal as well as for the complexes in solution (data not shown). These findings clearly indicate that the characteristics of the protein crystal depend critically on the experimental conditions of its preparation and suggest that the micro-Raman technique may offer a sensitive tool for the screening of sample preparation.

The laser power at the sample might also be a parameter to fine-tune to avoid artifacts. In this particular case, the amount of the 6c LS heme depends on the laser power at the sample surface during the RR experiment. For single crystals of ARP/CIP-BHA soaked in $(NH_4)_2SO_4$, the higher the laser power, the greater the intensity of the bands characteristic of the 6c LS (Figure 6B). A laser power of 550 μW on the crystal gave rise to an almost pure 6c LS heme with core size marker bands at 1551 cm^{-1} (ν_{38}), 1565 cm^{-1} (ν_{11}), 1587 cm^{-1} (ν_{19}), and 1639 cm^{-1} (ν_{10}) (Figure 6B, spectrum c). The band at 1624 cm^{-1} is assigned to the ν(C═C) vinyl stretching mode as for wild type (*40*), indicating that the orientation of the vinyl substituents is not influenced by the coordination and spin state changes. At low laser power, without taking into account the 6c LS species, the relative amount of the 5c and 6c HS species observed in the ARP/CIP-BHA and ARP/CIP-SHA crystals soaked in the presence of $(NH_4)_2SO_4$ appears to be very similar to that observed in the crystals soaked in $(Na)_2SO_4$. At high laser power, the 6c LS species formed during irradiation seems to derive from the 6c HS species. The spin state of the ARP/CIP-BHA and SHA complexes in solution containing $(NH_4)_2SO_4$ were also found to be laser power dependent (data not shown).

The X-ray crystal structure of ARP/CIP-BHA in the absence of $(NH_4)_2SO_4$ was solved (data not shown). However, a comparison of the $2F_0 - F_c$ and $F_0 - F_c$ maps around the heme of ARP/CIP-BHA in ammonium sulfate (*4*) and in sodium acetate reveals very similar electron densities. In both structures, using different restraints, the distance between the heme iron and the distal water molecule W801 is found to be 2.6 Å. Therefore, the X-ray data cannot help in attempting to understand the nature of the sixth ligand in the low spin species. Nevertheless, since the 6c LS species appears to be present only in the crystals soaked in solution containing $(NH_4)_2SO_4$, it cannot be excluded that NH_3 binds to the heme Fe since it is well-known that NH_3 is able to bind the ARP/CIP heme iron at mild alkaline pH (*26*). Figure 7 highlights the effect of $(NH_4)_2SO_4$ on the coordination state of ARP/CIP at pH 8.0. It can be seen that whereas the protein in solution without $(NH_4)_2SO_4$ gives rise to a spectrum (Figure 7, spectrum a) identical to that shown in Figure 5 at pH 5.5, and therefore, typical of a pure 5c HS heme, upon addition of $(NH_4)_2SO_4$, the low spin heme appears in both the crystal and the solution spectra (Figure 7, spectra b and c). In this case, no effect induced by the laser power was observed. In addition, the 6c LS heme is evident in the corresponding electronic absorption spectrum prior to laser irradiation as previously reported (*26*).

CONCLUSIONS

The comparison of RR spectra of resting state and ligand bound ARP/CIP in solution and single crystal form indicates that the coordination state can be dramatically affected by the physical or chemical conditions. In particular, the crystals

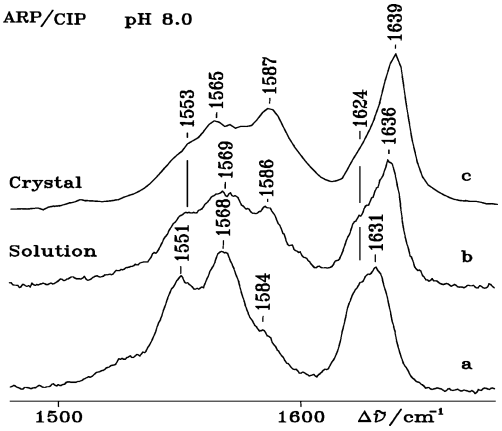

FIGURE 7: Effect of $(NH_4)_2SO_4$ on the coordination state of ARP/CIP. Resonance Raman spectra of ARP/CIP at pH 8.0 in solution (a and b) and as a single crystal (c) with $(NH_4)_2SO_4$ (b and c) and without $(NH_4)_2SO_4$ (a). Experimental conditions: 514.5 nm excitation; 5 cm^{-1} spectral resolution. (a) 2.3 mW laser power at the sample, 600 s accumulation time; (b) 2.8 mW laser power at the sample, 600 s accumulation time; and (c) 130 μW laser power on the crystal surface, 1800 s accumulation time.

soaked in solution containing $(NH_4)_2SO_4$ are characterized by the presence of a 6c LS heme; however, the nature of the sixth ligand could not be identified by the X-ray determination.

In the absence of $(NH_4)_2SO_4$ and at pH 5.5, only minor differences between the solution and the crystalline states are observed both for the free protein and for the SHA or BHA complexes. These differences can be ascribed to a striking enhancement of the inversely polarized ν_{19} mode, deriving from a larger ruffled distortion of the heme of the resting and ligand bound ARP/CIP crystals with respect to the solutions.

Upon addition of SHA or BHA, the protein partially converts to a 6c HS heme; however, the ARP/CIP-BHA and SHA binding profiles indicate the presence of one binding site for BHA and two binding sites for SHA. The SHA binding site at lower affinity does not affect the spin and coordination state of the heme iron.

The combined analysis of the spectroscopic data and X-ray crystal structures of the ARP/CIP-SHA complex indicates that the Fe−H_2O distance as measured by X-ray diffraction is an average resulting from the 5c and 6c species in equilibrium that, however, are directly revealed by RR spectroscopy.

ACKNOWLEDGMENT

We thank Drs. Mamoru Suzuki and Noriyuki Igarashi of the Photon Factory for their help with data collection using synchrotron radiation, Masakazu Sugishima for processing the diffraction images, and Drs. N. C. Veitch (Jodrell Laboratory, Kew, UK) and A. Feis (Università di Firenze, I) for helpful discussions. We are grateful to Prof. K. G. Welinder (Aalborg University, DK) for the generous gift of purified CIP.

REFERENCES

1. Henriksen, A., Schuller, D. J., Meno, K., Welinder, K. G., Smith, A. T., and Gajhede, M. (1998) *Biochemistry 37*, 8054−8060.
2. Smulevich, G., Neri, F., Marzocchi, M. P., and Welinder, K. G. (1996) *Biochemistry 35*, 10576−10585.
3. Kjalke, M., Andersen, M. B., Schneider, P., Christensen, B., Schülein, M., and Welinder, K. G. (1991) *Biochim. Biophys. Acta 1120*, 248.
4. Itakura, H., Oda, Y., and Fukuyama, K. (1997) *FEBS Lett. 412*, 107−110.
5. Tsukamoto, K., Itakura, H., Sato, K., Fukuyama, K., Miura, S., Takahashi, S., Ikezawa, H., and Hosoya, T. (1999) *Biochemistry 38*, 12558−12568.
6. Davey, C. A., and Fenna, R. E. (1996) *Biochemistry 35*, 10967−10973.
7. Schonbaum, G. R. (1973) *J. Biol. Chem. 248*, 502−511.
8. Teraoka, J., and Kitagawa, T. (1980) *J. Phys. Chem. 84*, 1928−1935.
9. Kitagawa, T., Hashimoto, S., Teraoka, J., Nakamura, S., Yajima, H., and Hosoya, T. (1983) *Biochemistry 22*, 2788−2792.
10. Smulevich, G., English, A., Mantini, A. R., and Marzocchi, M. P. (1991) *Biochemistry 30*, 772−779.
11. Howes, B. D., Rodriguez-Lopez, J. N., Smith, A. T., and Smulevich, G. (1997) *Biochemistry 36*, 1532−1543.
12. Gupta, R. K., Mildvan, A. S., and Schonbaum, G. R. (1979) *Biochem. Biophys. Res. Comm. 89*, 1334−1340.
13. deRopp, J. S., Mandal, P., Brauer, S. L., and La Mar, G. N. (1997) *J. Am. Chem. Soc. 119*, 4732−4739.
14. Smulevich, G., English, A. M., Mantini, A. R., and Marzocchi, M. P. (1991) *Biochemistry 30*, 772−779.
15. Smulevich, G., Feis, A., Indiani, C., Becucci, M., and Marzocchi, M. P. (1999) *J. Biol. Inorg. Chem. 4*, 39−47.
16. Indiani, C., Feis, A., Howes, B. D., Marzocchi, M. P., and Smulevich, G. (2000) *J. Am. Chem. Soc. 122*, 7368−7376.
17. Altose, M. D., Zheng, Y., Dong, J., Palfey, B. A., and Carey, P. R. (2001) *Proc. Natl. Acad. Sci. U.S.A. 98*, 3006−3011.
18. Smulevich, G. (1998) *Biospectroscopy 4*, S3−S17.
19. Dalbøge, H., Jensen, E. B., and Welinder, K. G. (1992) Patent application WO 92/16634.
20. Smulevich, G., Feis, A., Focardi, C., and Welinder, K. G. (1994) *Biochemistry 33*, 15425−15432.
21. Kunishima, N., Fukuyama, K., Wakabayashi, S., Sumida, M., Takaya, M., Shibano, Y., Amachi, T., and Matsubara, H. (1993) *Proteins: Struct., Funct., Genet. 15*, 216−220.
22. Wariishi, H., Nonaka, D., Jojima, T., Nakamura, N., Naruta, Y., Kubo, S., and Fukuyama, K. (2000) *J. Biol. Chem. 275*, 32919−32924.
23. Andersen, M. B., Hsuanyu, Y., Welinder, K. G., Schneider, P., and Dunford, H. B. (1991) *Acta Chem. Scand. 45*, 206−211.
24. Leslie, A. G. W. (1992) *Joint CCP4 and ESF-EACBM Newsletter on Protein Crystallography*, Daresbury Laboratory, Warrington, UK.
25. Collaborative Computational Project (1994) *Acta Crystallogr. D50*, 760−763.
26. Kunishima, N., Amada, F., Fukuyama, K., Kawamoto, M., Matsunaga, T., and Matsubara, H. (1996) *FEBS Lett. 378*, 291−294.
27. Roussel, A. C. C. (1992) *Silicon Graphycs Geometry Directory*, Silicon Graphycs, Mountain View, CA.
28. Hamilton, W. C., Rollett, J. S., and Sparks, R. A. (1965) *Acta Crystallogr. 18*, 129−130.
29. Henry, E. H., and Hofrichter, J. (1992) *Methods Enzymol. 210*, 129−155.
30. Henriksen, A., Mirza, O., Indiani, C., Teilum, K., Smulevich, G., Welinder, K. G., and Gajhede, M. (2001) *Protein Sci. 10*, 108−115.
31. Gajhede, M., Schuller, D. J., Henriksen, A., Smith, A. T., and Poulos, T. L. (1997) *Nat. Struct. Biol. 4*, 1032−1038.
32. Veitch, N. C., Williams, R. J. P., Bone, N. M., Burke, J. F., and Smith, A. T. (1995) *Eur. J. Biochem. 233*, 650−658.
33. Veitch, N. C., Gilfoyle, D. J., White, C. G., and Smith, A. T. (1996) in *Plant peroxidases*: *Biochemistry and Physiology* (Obinger, C., Burner, U., Ebermann, R., Penel, C., and Greppin, H., Eds.) pp 1−6, University of Geneva, Geneva, Switzerland.
34. Veitch, N. C., Gao, Y., Smith, A. T., and White, C. G. (1997) *Biochemistry 36*, 14751−14761.
35. Aitken, S. M., Turnbull, J. L., Percival, M. D., and English, A. (2001) *Biochemistry 40*, 13980−13988.
36. Smulevich, G., Feis, A., Indiani, C., Becucci, M., and Marzocchi, M. P. (1999) *J. Biol. Inorg. Chem. 4*, 39−47.
37. Indiani, C., Feis, A., Howes, B. D., Marzocchi, M. P., and Smulevich, G. (2000) *J. Am. Chem. Soc. 122*, 7368−7376.
38. Bonamore, A., Farina, A., Gattoni, M., Schininà, E., Bellelli, A., and Boffi, A. (2003) *Biochemistry 42*, 5792−5801.

39. Choi, S., Spiro, T. G., Langry, K. C., Smith, K. M., Budd, D. L., and La Mar, G. N. (1982) *J. Am. Chem. Soc. 104*, 4345−4351.
40. Smulevich, G., Feis, A., Focardi, C., Tams, J., and Welinder, K. G. (1994) *Biochemistry 33*, 15425−15432.
41. Howes, B. D., Schiodt, C. B., Welinder, K. G., Marzocchi, M. P., Ma, J. G., Zhang, J., Shelnutt, J. A., and Smulevich, G. (1999) *Biophys. J. 77*, 478−492.
42. Smulevich, G., Wang, Y., Mauro, J. M., Wang, J. M., Fishel, L. A., Kraut, J., and Spiro, T. G. (1990) *Biochemistry 29*, 7174−7180.
43. Wang, J., Mauro, J. M., Edwards, S. L., Oatley, S. J., Fishel, L. A., Ashford, V. A., Xuong, N., and Kraut, J. (1990) *Biochemistry 29*, 7160−7173.
44. Brünger, A. T. (1992) *X-PLOR, version 3.1*, Yale University, New Haven, CT.

BI035290L